



## Effect of microstructure and crystallographic texture on the Charpy impact test for maraging 300 steel

Mohammad Masoumi <sup>\*</sup>, Isabel Ferreira de Barros, Luis Flavio Gaspar Herculano, Hana Livia Frota Coelho, Hamilton Ferreira Gomes de Abreu

Department of Metallurgical and Materials Engineering, Federal Universidade of Ceará, Fortaleza, CE, Brazil

### ARTICLE INFO

#### Article history:

Received 27 May 2016

Received in revised form 9 August 2016

Accepted 5 September 2016

Available online 6 September 2016

#### Keywords:

Solution annealing temperatures

Impact toughness

Crystallographic orientation

### ABSTRACT

The effect of different solution annealing temperatures on the hardness, impact toughness and crystallographic orientation of high strength martensitic 300 grade maraging steel was investigated. The results showed that the solution annealing temperature has a significant influence on the impact toughness energy because of the engineering of the crystallographic textures. The impact toughness improved with increasing intensity of the {111}, {112} and {110}//ND (normal direction) fibres up to approximately 1000 °C in solution annealing. The Charpy impact energy reached a maximum without any significant loss in hardness for the discussed conditions. However, solution annealing at 1100 °C developed an undesirable rotated cubic texture component because of the recrystallised cubic component in the austenite grains, which led to a significant reduction in impact toughness energy.

© 2016 Elsevier Inc. All rights reserved.

### 1. Introduction

High strength martensitic 300 grade maraging steel with minor additions of titanium, aluminum and chromium exhibits an excellent combination of strength and toughness by the precipitation hardening mechanism during solution treatment and subsequent aging [1,2]. These alloys have been widely used in many industrial applications, such as aerospace, high-performance shafting, electric motors and aircraft. Furthermore, the production of magnets for high-speed rotors is one of the main applications of these steels. However, the magnetic properties generally cannot be combined with desirable mechanical properties [3].

Heat treatment processing plays a significant role in controlling the mechanical properties of high strength 300 grade maraging steel. Significant attention has been paid to investigating the effect of solution treatment and aging behaviour of these steels over recent decades [4–6]. Hardening treatment of these steels consists of solution annealing followed by an aging processing for 1–4 h. It has been reported that the highest yield stress levels are achieved after aging for 1 h at 480 °C, due to the precipitation of intermetallic compounds, such as Ni<sub>3</sub>Ti, Ni<sub>3</sub>Mo, Fe<sub>2</sub>Mo and Fe<sub>7</sub>Mo<sub>6</sub> [7,8]. In general, the formation of reverted austenite during aging improves the tensile and toughness properties [9,10]. It is expected that metastable retained/reverted austenite leads to larger elongation due to the austenite to martensite transformation during deformation [11,12]. The volume fraction and morphology of the retained/reverted austenite can also affect the final mechanical

properties which depend on the time and temperature of the heat treatment. Since the mechanical behaviour and deformation mechanisms of steels are extremely dependent on the initial texture, it is important to evaluate the mechanical behaviour and microstructural evolutions of these steels under different aging temperatures.

In maraging steels, the austenitic structure transforms to a body centred cubic (BCC) martensite by shearing, which is softer and tougher than the ordinary body centred tetragonal (BCT) martensite, during cooling even when the cooling rate is very low [13]. The mechanism of martensite formation in iron-nickel alloys has been studied in a great number of works [14–16]. Unlike the austenite-ferrite changes in common steels, maraging steels containing at least 18% Ni do not decompose into equilibrium austenite and ferrite at around 450 °C. Instead, with further cooling, the austenite transforms to martensite with a BCC structure. Also, maraging steel with very low carbon content and several percent titanium tends to precipitate any traces of these interstitials in the alloy, thus removing them from the solid solution [17]. The lattice distortion in the structure leads to weakening of the covalent bonds, especially in the {001} planes with a low number of nearest neighbours and low dense atomic packing planes. As a consequence, grains oriented with {001} provide an easier path for crack propagation, leading to a significant reduction in toughness. In BCC steels, the {001}{110} (rotated cube) texture component in the ferrite phase is generated from the recrystallised {001}{010} (cube) component in the austenite phase, which is known as a cleavage plane [18,19]. Alternatively, based on dislocation theories and Taylor factor analyses, it has been shown that crystallographic orientations associated with {110}, {111} and {112}, corresponding to the close-packed plane in the BCC structure, show higher mechanical and toughness properties [20,21].

<sup>\*</sup> Corresponding author.

E-mail address: [mohammad@alu.ufc.br](mailto:mohammad@alu.ufc.br) (M. Masoumi).

Therefore, particular attention to crystallographic orientations is required to obtain excellent mechanical properties.

Crystallographic orientations and grain boundary characteristics can influence the Charpy impact energy. Texture can increase the toughness by providing enough available slip systems to enhance dislocation movement to improve ductility [22]. Grain boundaries can act as obstacles to crack propagation, while the undesirable cleavage {001}//ND grains facilitate crack propagation and decrease the toughness. The main purpose of the present investigation was to determine the influence of the preferred crystallographic orientations on the toughness fracture properties in high strength martensitic 300 grade maraging steel under different solution annealing temperatures. Experimental results demonstrate that the fracture toughness and hardness behaviour were influenced by some metallurgical parameters, such as the prior austenite volume fraction, grain size and crystallographic orientations.

## 2. Materials and Methods

An ingot of high strength martensitic 300 grade maraging steel, produced by a vacuum induction melting process (VIM), followed by a vacuum arc refining process (VAR), was used in this work. The chemical composition of the steel is given in Table 1. The top and bottom of the ingot were cut and the surface was machined to remove surface defects. The ingot with a diameter of 250 mm was firstly forged down to a round bar, 150 mm in diameter. Rectangular materials with 30 mm thicknesses were cut from the bar and hot rolled at 1000 °C to sheet with 10 mm in a thick sheet. Next, the rolled sheet was cut and subjected to different solution annealing treatments at temperatures of 860, 900, 950, 1000, 1050, 1100 and 1150 °C for 1 h, followed by water quenching to room temperature. Then, aging for 3 h at a temperature of 480 °C was conducted to produce a fine dispersion of Ni<sub>3</sub>Ti intermetallic phases along dislocations left by the martensitic transformation [23,24] to provide an excellent combination of mechanical and toughness properties.

The microstructural examination was performed using a ZEISS Axio Imager 2 on the rolling plane of the specimens. The samples were ground using SiC papers up to 1200, polished with 6, 3 and 1 µm diamond paste and finally etched with an ammonium persulfate ((NH<sub>4</sub>)<sub>2</sub>S<sub>2</sub>O<sub>8</sub>) reagent to reveal the structure. Moreover, the samples were etched by 2% Nital to reveal the prior-austenite grain boundaries. The evaluation of the average grain size was completed by measuring the diameter of the equivalent area with individual grains using Image-Pro software on an Olympus optical BX51M microscope. Furthermore, Vickers micro-hardness measurements were performed on the specimens.

The Charpy impact test on rectangular sub-sized Charpy V-notch specimens parallel to the transverse direction of 55 mm × 10 mm × 7.5 mm (transverse × rolling × thickness direction), which was expected to be the lowest Charpy value, was conducted at room temperature by a WPM Leipzig pendulum impact tester of 500 J capacity (model: PSd 150, Markkleeberg, Germany). Then, X-ray diffraction (XRD) using a Panalytical X-Pert diffractometer equipped with monochromatic Cu Kα radiation was performed at mid-thickness of the specimens to investigate the reverted austenite in the specimens.

To study the role of crystallographic orientation on the plastic deformation at various solution annealing temperatures, the orientation distribution function (ODF) at mid-thickness of the specimens was analysed. Three incomplete pole figures, i.e. {110}, {200}, and {211}, were obtained in the reflection mode on a 5° grid up to an 85° sample tilt. Then, the related ODF was determined by MTEX – free and open source software toolbox. The electron backscatter diffraction (EBSD)

measurements were conducted in a plane perpendicular to the transverse direction of the sheet. EBSD data were acquired using a Phillips XL30 scanning electron microscope operating at an acceleration voltage of 20 kV, sample tilt angle of 70°, working distance of 12 mm and a 0.5 µm step size. HKL Channel 5 software was used to analyse the EBSD data.

## 3. Results and Discussion

### 3.1. Microstructure and Hardness

The optical micrographs of specimens under different solution annealing treatments for 1 h, followed by aging at 480 °C for 3 h, are shown in Fig. 1. The BCC martensite formed by shear deformation due to rapid cooling of the austenite phase was found in the microstructure. The microstructures also demonstrate packets of lath martensite with a high dislocation density that is typically formed in these steels during solution annealing, followed by aging treatments. The purpose for different solution annealing temperatures was to obtain the different particle dissolution conditions and lath martensite types and regions of dislocation cell-type martensite due to the variation of the prior austenite grains. It was observed that the prior austenite grains significantly grew by increasing the solution annealing temperature. This can influence the martensite transformation and results in significant differences in the microstructure and mechanical properties, as shown later in the manuscript.

The effect of solution annealing temperature on the prior austenite grain size and hardness is shown in Fig. 2. The results demonstrated that the grain growth of the prior austenite grains was negligible up to 1050 °C, while a significant grain growth was observed at solution annealing temperatures higher than 1100 °C. It is known that grain growth are controlled by grain boundary pinning and finely dispersed second phase particles [25]. It is well-known that a new set of austenite grains formed at a large number of sites during annealing, especially at grain boundaries. Since the austenite transformation was completed, the average grain sizes of austenite increased with solution annealing temperature, from about 6 µm to 190 ± 15 µm for 860 to 1150 °C annealing temperatures, respectively. At the grain growth step, some larger austenite grains kept growing at the expense of the smaller ones, leading to a decrease in the number of grains. However, the reduction in total grain boundaries in austenite grains provides a driving force for the grain growth [26]. The precipitation hardening mechanism was eliminated due to the second phase dissolution during annealing at very high temperature.

Fig. 2b presents the variation of hardness on different solution annealing temperatures. The hardness decreased generally with increasing prior austenite grain sizes by increasing the annealing temperature, which is in agreement with the Hall-Pitch relationship regarding the concept that grain boundaries hinder dislocation movement. However, a peak in hardness in the 1000 °C solution was found. Then, the reverted austenite characterised during solution annealing at 1150 °C, followed by aging treatment, enhanced the hardness reduction, as shown in Fig. 2b.

### 3.2. Charpy Impact Energy

Fig. 3 presents the results of the Charpy impact energy tests carried out on the investigated samples. The results showed the impact energy dependence on the temperature of the solution annealing treatment. According to the Hall-Pitch equation, smaller grain sizes possess higher resistance to brittle cleavage fracture since grain boundaries are effective barriers to the propagation of brittle fractures [27]. Although, the results of the impact test proved the existence of an optimum solution annealing temperature in the energy of the impact test. This energy was increased gradually to reach a maximum at 1000 °C, then, a slight decrease was observed at 1050 °C, and the energy of the Charpy impact

**Table 1**  
Chemical composition of high strength 300 grade maraging steel.

Element	Ni	Mo	Co	Ti	Al	C	Mn	Si	Fe
wt.%	18,4	5,04	9,35	0,76	0,12	0,01	0,02	0,05	Bal.

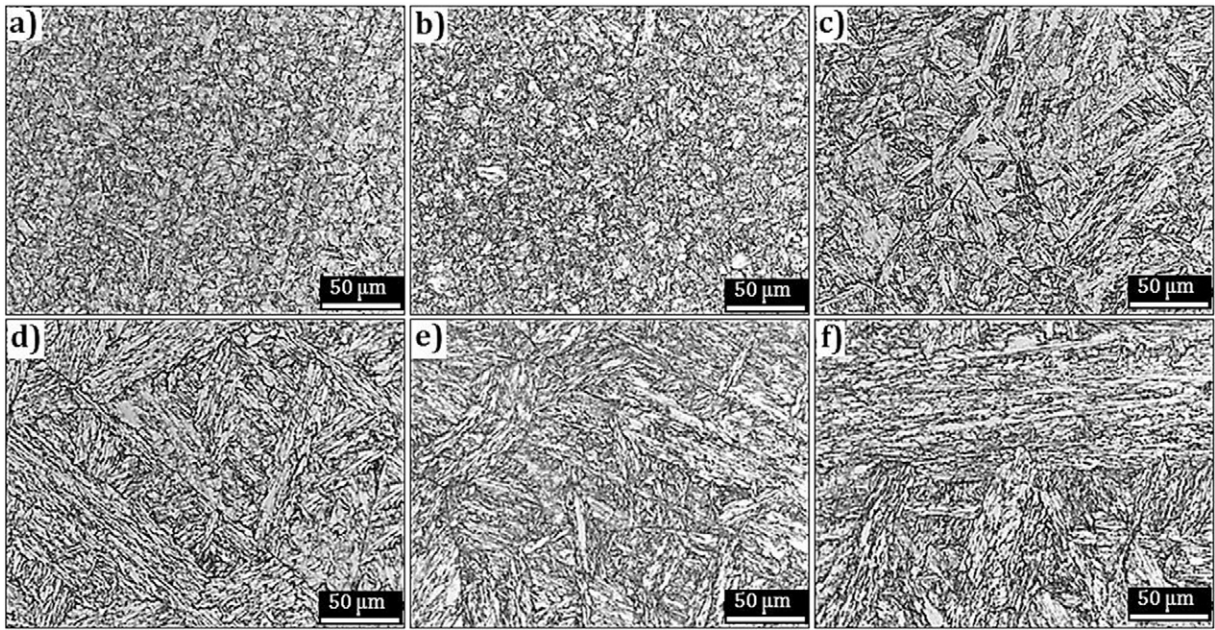


**Fig. 1.** Micrographs of specimens at different solution-annealing temperatures at, a) 900 °C, b) 950 °C, c) 1000 °C, d) 1050 °C, e) 1100 °C, and f) 1150 °C for 1 h, followed by aging at 480 °C for 3 h.

energy test dropped dramatically to the minimum amount. Finally, solution annealing treatment at 1150 °C leads to an increase in the absorbed energy during the Charpy impact energy test due to the retained austenite phase formation.

XRD analysis was conducted in the centre region of the specimens to provide information about the microstructure and phase transformation (Fig. 4). The steel was completely martensitic at room temperature, up to a solution annealing temperature at 1100 °C. The XRD patterns obtained from the sample treated by 1150 °C solution annealing illustrated that about 20% retained austenite was found in this condition without transforming into martensite during water quenching. Podder et al. [28] reported that solution annealing higher than a critical temperature leads to a redistribution of alloying elements between the martensite laths and austenite phase dispersed. The enrichment austenite phase of Ni, carbon and other alloying elements was developed by the dissolution of the precipitates in the matrix. Therefore, the martensite start ( $M_s$ ) temperature shifts to below room temperature at higher concentrations of alloying elements. This soft austenite phase absorbs more energy generated by the Charpy test and increases the ductility. In other words, retained austenite in the matrix transforms partly or entirely to martensite because of the transformation induced plasticity effect [29,30] during the Charpy test. Finally, the austenite phase remains

stable at room temperature after water quenching. This phase transformation and development of the hard martensite phase led to increasing toughness.

### 3.3. Texture Evolution

As a result of the similar microstructures obtained from all treatments, the variation in Charpy energy may result in differences in the crystallographic textures produced via different solution annealing temperatures. Therefore, macrotexture measurements were carried out at the mid-thickness of specimens and the related ODF at  $\varphi_2 = 45^\circ$  are presented in Fig. 5. The results demonstrated that the solution annealing temperature range of 860 to 1000 °C developed the {110}, {111}/ND fibres through the materials. It is believed that grains oriented with {111} and {110} have higher strengths and mechanical properties due to activated slip systems in the BCC structure [31]. Therefore, the good toughness in these solution annealing conditions is expected to develop the desired texture components. It is worth mentioning that the {112}  $\langle 1\bar{1}0 \rangle$  component was produced by shear deformation due to the water quenching at elevated temperatures in the austenite grains. The solution annealing at the FCC austenite phase with low

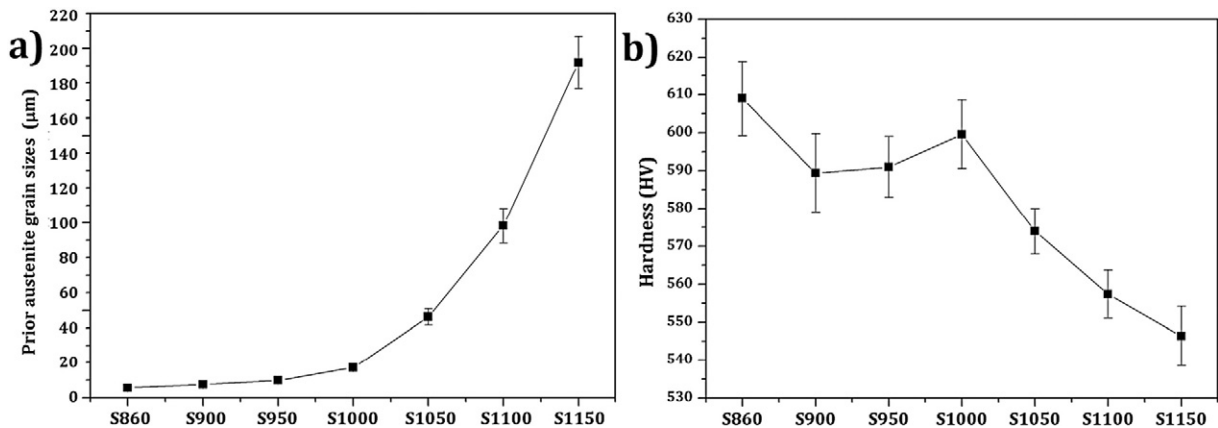


**Fig. 2.** (a) prior-austenite grain sizes and (b) Vickers micro-hardness measurements on different solution-annealing temperatures.

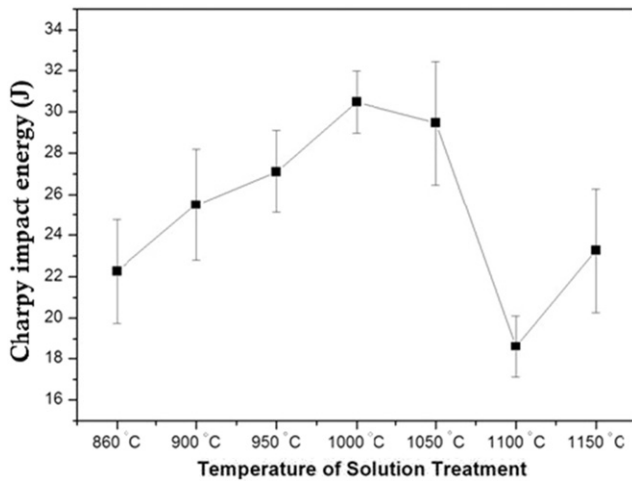


Fig. 3. Charpy impact energy on different solution-annealing temperatures.

stacking fault energy (SFE) developed  $\{110\}$ //ND fibre components, spreading from  $\{110\}\langle 443 \rangle$  to  $\{110\}\langle 1\bar{1}15 \rangle$ , which is about  $5^\circ$  away from the ideal orientation of the Goss component ( $\{110\}\langle 001 \rangle$ ) rotated about the normal direction [32]. Thus, a dislocation gliding on  $\{110\}$  planes dominated in this range of solution annealing temperatures.

Crystallographic analysis demonstrated that the dominant  $\{001\}$  and  $\{110\}$ //ND fibre components developed under solution annealing at  $1100^\circ\text{C}$ . Tóth et al. [33] reported that the  $\{100\}\langle 0\bar{1}0 \rangle$  (cube) component is dominant in the austenite phase due to low SFE, transforming into the  $\{100\}\langle 1\bar{1}0 \rangle$ ,  $\{100\}\langle \bar{1}\bar{1}0 \rangle$ ,  $\{110\}\langle 1\bar{1}0 \rangle$  and  $\{110\}\langle 001 \rangle$  (rotated cube, Goss and rotated Goss, respectively) components. The harmful effects on the discussed crystallographic orientation on a reduction of fracture toughness and mechanical properties were reported. The close random texture appearing as a result of solution annealing above  $1150^\circ\text{C}$  may cause high grain growth in the austenite phase. Recently, Kubota et al. [34] studied the recrystallisation behaviour of 0.55C (wt.%) steel. They suggested that the FCC-austenite to BCC-martensite transformation causes the compression parallel to a  $\langle 100 \rangle$  direction, the main orientation of the martensite particles was approximately parallel to an FCC  $\langle 110 \rangle$  direction [35]. This fibre became weaker during the recrystallisation of the austenite phase.

It could be concluded that the increase in the toughness behaviour was associated with increasing the orientation of  $\{111\}$ ,  $\{112\}$  and

$\{110\}$ //ND. Further, it is in agreement with the observation of the Young's modulus of steel, in which the  $\langle 111 \rangle$  direction has the highest modulus of iron [36]. It is notable that the  $\langle 112 \rangle$  direction is very close to the  $\langle 111 \rangle$  direction. In contrast, the  $\{001\}$ //ND preferred cleavage planes in steels have the lowest modulus, decreasing the Charpy energy in the specimen solution annealed at  $1100^\circ\text{C}$ .

### 3.4. EBSD Studies

The EBSD technique provides efficient data of the geometry of the lattice planes in the crystal, crystallographic orientation of the grain, grain boundaries and any other interesting information for better understanding the behaviour of the crystallographic structure during processing. In order to provide precise information about decreasing the toughness above  $1000^\circ\text{C}$  solution annealing, EBSD measurements were carried out in two annealed specimens at  $1000^\circ\text{C}$  and  $1100^\circ\text{C}$ . Fig. 6 shows EBSD orientation maps of the specimens. The medium angle grain boundaries (MAGBs) with a point-to-point misorientation between  $5$  and  $15^\circ$  and high angle grain boundaries (HAGBs) with misorientations  $> 15^\circ$  are marked as thin and thick black lines. The effects of different solution annealing temperatures on individual grain orientations, local texture and point-to-point misorientation angle were investigated separately as follows.

The orientation of grains in the specimens was demonstrated by normal direction inverse pole figures in Fig. 7. Fig. 7a showed the development of  $\{112\}$  and  $\{113\}$ //ND texture components in the EBSD analysis on the specimen annealed at  $1000^\circ\text{C}$ . The results were in agreement with previous findings on macro-texture studies, which showed that the  $\{112\}$  crystal plane, close to the compact  $\langle 111 \rangle$  direction in the BCC lattice provided the good toughness properties. Conversely, the reduction in impact toughness test at  $1100^\circ\text{C}$  was related to the increasing number of grains oriented with  $\{001\}$  planes parallel to the normal direction (Fig. 7b). It was shown that the strengthening of the undesirable components led to a reduction in fracture toughness. Therefore, the presence of grains oriented along  $\{001\}$ //ND promotes brittle behaviour during crack initiation and reduces ductility.

It is worth mentioning that the adjacent grains have different lattice orientations (misorientation) in tempered martensitic structure can control the energy of toughness [37]. Since dislocations cannot move by changing directions, the pile ups dislocation at grain boundaries happens, thus, the local stress concentration in the vicinity of grains is formed leading to provide an easier path for crack propagation. It is generally believed that low angle grain boundaries (LAGBs) with less stored energy show higher resistance to crack nucleation and

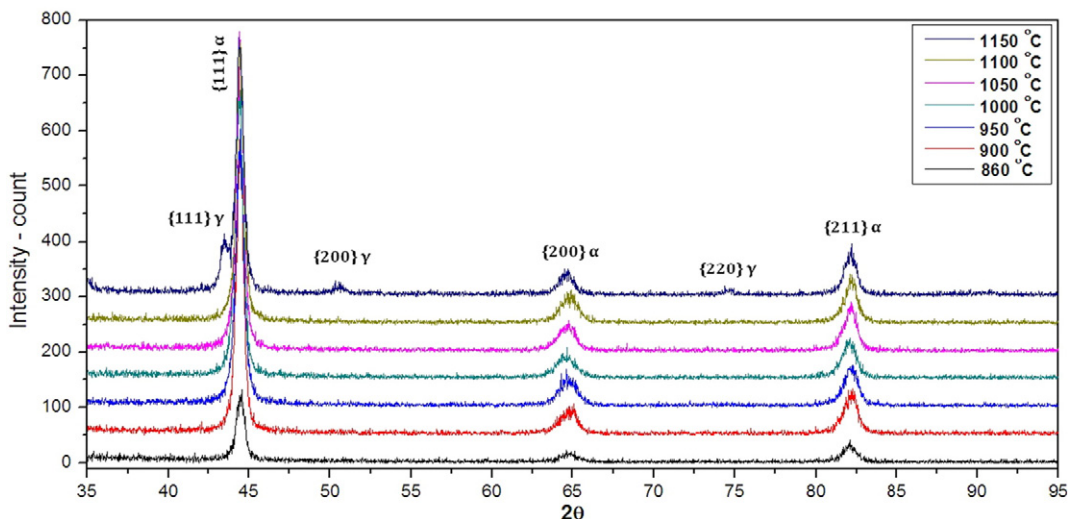


Fig. 4. XRD pattern of sample showing ferrite, retained austenite on different solution-annealing temperatures followed by aging at  $480^\circ\text{C}$ .

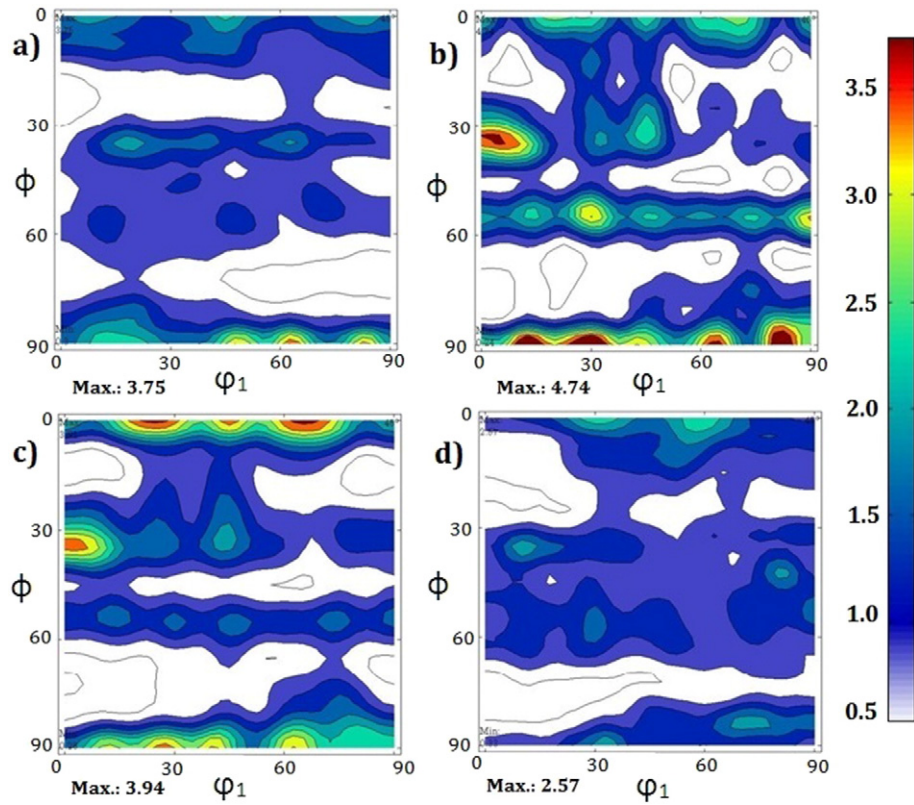


Fig. 5. ODF at  $\phi_2 = 45^\circ$  for a) 860, b) 1000, c) 1100, and d) 1150 °C solution-annealing temperature.

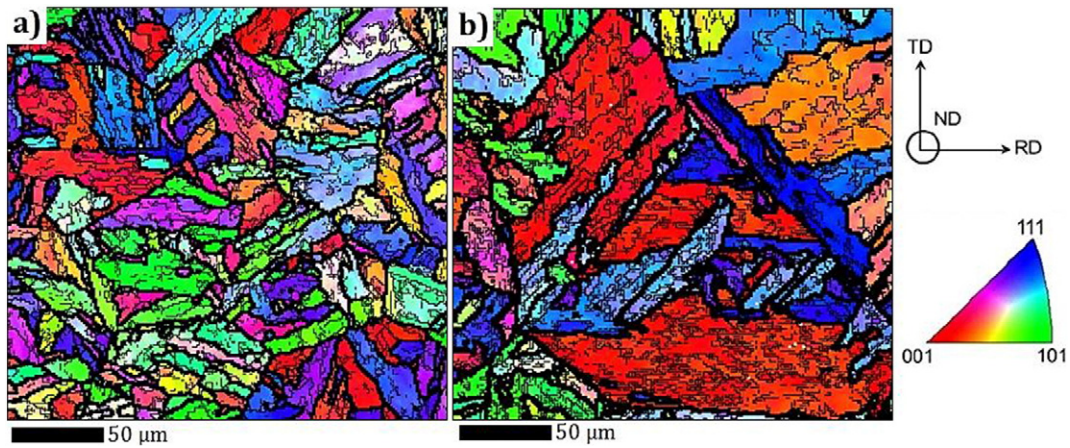


Fig. 6. EBSD orientation maps for (a) 1000 °C and (b) 1100 °C solution-annealing temperature.

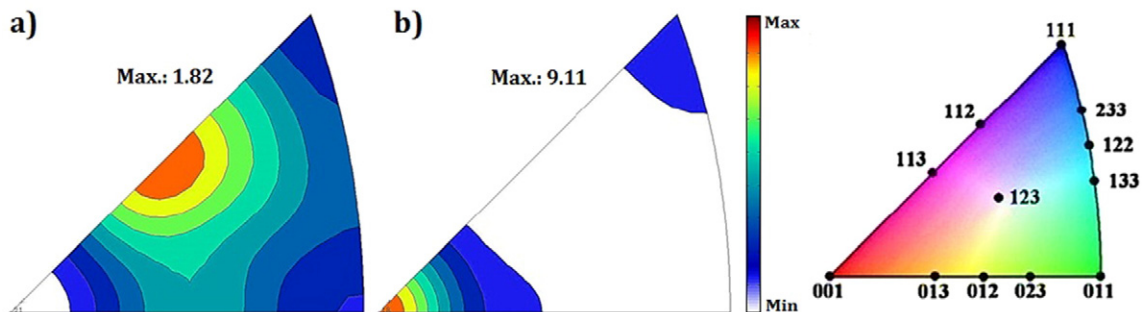


Fig. 7. Inverse pole figures for (a) 1000 and (b) 1100 °C solution-annealing temperature.

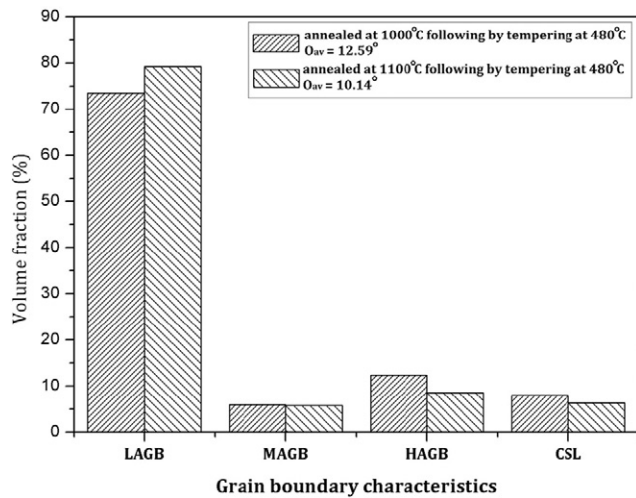


Fig. 8. Grain boundary distribution 1000 and 1100 °C solution-annealing temperature.

propagation, while HAGBs have lower resistance to crack formation due to the stored energy because of the higher incompatible lattice fit. However, the correlation of MAGBs and special grain boundary (CSL) distribution in specimens was negligible (Fig. 8). Recently, Gottschalk et al. [38] reported that the mismatch in the slip systems in adjacent grains may affect the deformation mechanism. From Fig. 8, it is observed that both annealing conditions showed a high volume of LAGBs. However, the grain boundaries in solution annealing at 1000 °C related to {112}, {113} and {110} (which are close to compact directions in the BCC lattice) had more resistance against the crack formation and failure behaviour, while LAGBs were observed in solution annealing at 1100 °C associated with the cleavage {001} planes, thus low toughness was found. In other words, more slip systems are expected to activate to facilitate dislocation movement, leading to improving ductility behaviour.

#### 4. Conclusions

The effects of crystallographic texture, retained austenite and prior austenite grain size on the energy of the impact test in high strength martensitic 300 grade maraging steel, subjected to different solution annealing temperatures, have been studied. The principal conclusion that can be drawn from the results is that it is feasible to improve the Charpy impact energy using crystallography texture control.

- The Charpy impact energy reached the maximum at 1000 °C without a significant loss in hardness.
- The energy of the Charpy impact test was increased with increasing {111}, {112}, and {110}//ND texture fibres up to approximately 1000 °C.
- Solution annealing at 1100 °C developed an undesirable rotated cubic component, leading to a significant reduction in impact toughness.
- Solution annealing at 1150 °C caused about 20% retained austenite that toughness performance relatively improved associated with work-hardening of retained austenite and austenite to martensite transformation even though the hardness decreased.
- The grain boundaries which are close to compact directions in the BCC lattice, such as {112}, {113} and {110}, showed more failure resistance rather than the boundaries related to the cleavage {001} planes.

#### Acknowledgments

The authors acknowledge the Coordenação de Aperfeiçoamento de Pessoal de Nível Superior (CAPES) (2974/2013) for financial support.

#### References

- [1] A. Markfeld, A. Rosen, The effect of reverted austenite on the plastic deformation of maraging steel, *Mater. Sci. Eng.* 46 (1980) 151–157.
- [2] A.G. Reis, D.A.P. Reis, A.J. Abdalla, J. Otubo, High-temperature creep resistance and effects on the austenite reversion and precipitation of 18 Ni (300) maraging, *Mater. Charact.* 107 (2015) 350–357.
- [3] A. Mahmoudi, M.R. Zamanzad Ghavidel, S. Hossein Nedjad, A. Heidarzadeh, M. Nili Ahmadabadi, Aging behavior and mechanical properties of maraging steels in the presence of submicrocrystalline Laves phase particles, *Mater. Charact.* 62 (2011) 976–981.
- [4] J. An, F. Meng, X. Lv, H. Liu, X. Gao, Y. Wang, Y. Lu, Improvement of mechanical properties of stainless maraging steel laser weldments by post-weld ageing treatments, *Mater. Des.* 40 (2012) 276–284.
- [5] H. Hou, H. Li, Y. Jin, X. Wang, Z. Wen, Effect of heat treatment temperature on the mechanical properties of low-temperature high strength maraging steel, *Mater. Sci. Eng. A* 601 (2014) 1–6.
- [6] V. Fuster, A.V. Druker, A. Baruj, J. Malarría, R. Bolmaro, Characterization of phases in an Fe–Mn–Si–Cr–Ni shape memory alloy processed by different thermomechanical methods, *Mater. Charact.* 109 (2015) 128–137.
- [7] E.M. Sherif, Corrosion inhibition in 2.0 M sulfuric acid solutions of high strength maraging steel by aminophenyl tetrazole as a corrosion inhibitor, *Appl. Surf. Sci.* 292 (2014) 190–196.
- [8] M. Ahmed, A. Ali, S.K. Hasnain, F.H. Hashmi, A.Q. Khan, Magnetic properties of maraging steel in relation to deformation and structural phase transformations, *Acta Metall. Mater.* 42 (1994) 631–638.
- [9] H.F.G. Abreu, S.S.M. Tavares, J.J.M. Silva, J.W.A. Menezes, A.D. Bruno, The influence of an intermediate austenitization heat treatment in the texture of cold-rolled and aged 18% Ni maraging, *Mater. Charact.* 52 (2004) 203–207.
- [10] W. Sha, Z. Guo, E.A. Wilson, Modeling the evolution of microstructure during the processing of maraging steels, *JOM* 56 (2004) 62–66.
- [11] M.A. Kenawy, M.R. Nagy, E.M. Sakr, Martensite-austenite transformation in maraging steel alloys during tensile deformation and thermal cycling, *J. Mater. Sci.* 21 (1986) 3071–3077.
- [12] B.C. De Cooman, Structure–properties relationship in TRIP steels containing carbide-free bainite, *Curr. Opin. Solid State Mater. Sci.* 8 (2004) 285–303.
- [13] R.F. Decker, Source book on maraging steels: a comprehensive collection of outstanding articles from the periodical and reference literature, *Am. Soc. Met.* (1979) 1–12.
- [14] U.K. Viswanathan, G.K. Dey, M.K. Asundi, Precipitation hardening in 350 grade maraging steel, *Metall. Trans.* 24A (1993) 2429–2442.
- [15] F.C. Campbell, *Manufacturing Technology for Aerospace Structural Materials*, Elsevier Sci. (2006) 171–185.
- [16] F. Qian, J. Sharp, W.M. Rainforth, Characterisation of L21-ordered Ni<sub>2</sub>TiAl precipitates in Fe single bond Mn maraging steels, *Mater. Charact.* 118 (2016) 199–205.
- [17] P.G. Shewmon, *Transformations in Metals* (McGraw-Hill Series in Materials Science & Engineering), McGraw Hill, 1969 340–343.
- [18] A.I. Haq, A.Q. Khan, The rolling texture of 18% Ni-350 maraging steel, *ASM Int.* (1993) 89–96 (JMPE 2).
- [19] P.K.C. Venkatsury, R.D.K. Misra, M.D. Mulholl, M. Manohar, J.E. Hartmann, Effect of microstructure on the mechanical properties and texture in high strength 560 MPa linepipe steels, *Mater. Sci. Eng. A* 575 (2013) 6–14.
- [20] R.K. Ray, J.J. Jonas, R.E. Hook, Cold rolling and annealing textures in low carbon and extra low carbon steels, *Int. Mater. Rev.* 39 (1994) 129–172.
- [21] U.F. Kocks, N. Tomé, H.R. Wenk, Texture and Anisotropy; Preferred Orientations in Polycrystals and Their Effect on Materials Properties, 2000 248–274.
- [22] G.J. Baczynski, J.J. Jonas, L.E. Collins, The influence of rolling practice on notch toughness and texture development in high-strength linepipe, *Metall. Mater. Trans. A* 30 (1999) 3045–3054.
- [23] N.R. Comins, J.B. Clark, *Specialty Steels and Hard Materials: Proceedings of the International Conference on Recent Developments in Specialty Steels and Hard Materials*, 1983 45–52.
- [24] Technical data sheet, Allvac, VASCOMAX® C-200/C-250/C-300/C-350 2014, pp. 2–12.
- [25] J. Moon, C. Lee, Pinning efficiency of austenite grain boundary by a cubic shaped TiN particle in hot rolled HSLA steel, *Mater. Charact.* 73 (2012) 31–36.
- [26] S.J. Lee, Y.K. Lee, Prediction of austenite grain growth during austenitization of low alloy steels, *Mater. Des.* 29 (2008) 1840–1844.
- [27] S.K. Lawrence, B.P. Somerday, N.R. Moody, D.F. Bahr, Grain boundary contributions to hydrogen-affected plasticity in Ni-201, *JOM* 66 (2014) 1383–1389.
- [28] A.S. Podder, H.K.D.H. Bhadeshia, Thermal stability of austenite retained in bainitic steels, *Mater. Sci. Eng. A* 527 (2010) 2121–2128.
- [29] S.S. Sohn, K. Choi, J.H. Kwak, N.J. Kim, S. Lee, Novel ferrite–austenite duplex light-weight steel with 77% ductility by transformation induced plasticity and twinning induced plasticity mechanisms, *Acta Mater.* 78 (2014) 181–189.
- [30] A.G. Mamalis, G.N. Haidemenopoulos, Aspects of ductility, toughness and formability of steel sheet in relation to transformation plasticity, *J. Mater. Process. Technol.* 30 (1992) 211–230.
- [31] M. Masoumi, L.P.M. Santos, I.N. Bastos, S.S.M. Tavares, M.J.G. da Silva, H.F.G. de Abreu, Texture and grain boundary study in high strength Fe–18Ni–Co steel related to hydrogen embrittlement, *Mater. Des.* 91 (2016) 90–97.
- [32] M. Nezakat, H. Akhiani, M. Hoseini, J. Szpunar, Effect of thermo-mechanical processing on texture evolution in austenitic stainless steel 316L, *Mater. Charact.* 98 (2014) 10–17.
- [33] L.S. Tóth, K.W. Neale, J.J. Jonas, Stress response and persistence characteristics of the ideal orientations of shear texture, *Acta Metall.* 37 (1989) 2197–2210.

- [34] M. Kubota, K. Ushioda, G. Miyamoto, T. Furuhashi, Analysis of recrystallization behavior of hot-deformed austenite reconstructed from electron backscattering diffraction orientation maps of lath martensite, *Scr. Mater.* 112 (2016) 92–95.
- [35] A.J. Bogers, W.G. Burgers, Partial dislocations on the {110} planes in the B.C.C. lattice and the transition of the F.C.C. into the B.C.C. lattice, *Acta Metall.* 12 (1964) 255–261.
- [36] F.J. Humphreys, U.K.M. Hatherly, *Recrystallization and related annealing phenomena*, Second edition, 2004 182–226.
- [37] M. Tikhonova, R. Kaibyshev, X. Fang, W. Wang, A. Belyakov, Grain boundary assemblies developed in an austenitic stainless steel during large strain warm working, *Mater. Charact.* 70 (2012) 14–20.
- [38] D. Gottschalk, A. McBride, B.D. Reddy, A. Javili, P. Wriggers, C.B. Hirschberger, Computational and theoretical aspects of a grain-boundary model that accounts for grain misorientation and grain-boundary orientation, *Comput. Mater. Sci.* 111 (2016) 443–459.